Chapter 13

Damage Estimation of a Steel-Framed Building under Tsunami Flow Occurring after Earthquake

Daigoro Isobe and Seizo Tanaka

Additional information is available at the end of the chapter

http://dx.doi.org/10.5772/intechopen.76602

Abstract

The Great East Japan Earthquake and the following tsunami that occurred on March 11, 2011 caused a significant disaster along the ocean side of the Tohoku area. The big tsunami carried different kinds of debris such as ships and cars up the stream, which caused additional damage to the buildings in the area. In this chapter, a finite element approach for the damage estimation of a steel-framed building under tsunami flow is described. A seismic wave recorded during the earthquake was first applied to the model, followed by an input of fluid forces owing to the tsunami wave. A three-dimensional free-surface-flow analysis code based on the volume of fluid (VOF) method was adopted to simulate wave propagation problems and compare the obtained wave forces between several inflow conditions and building shapes. Then, a debris model with a velocity was collided, and the collapse behavior of the building was simulated using the adaptively shifted integration (ASI)-Gauss code.

Keywords: damage estimation, steel-framed building, tsunami, earthquake, VOF method, ASI-gauss code, fluid analysis, collapse analysis, finite element method

1. Introduction

A huge disaster occurred after the Great East Japan Earthquake on March 11, 2011, when the following big tsunami washed away most of the man-made structures in its way (**Figure 1**). The design and construction of tsunami evacuation buildings started soon after the event, particularly in areas where no other natural evacuation points were in the vicinity.

In this chapter, the wave forces owing to a tsunami acting on the surface of a building were evaluated by fluid analysis using the finite element method (FEM). Then, a one-way coupling

Figure 1. View of disaster site (Ishinomaki-shi, 2 weeks after the event) (photo by Katsunori Shoji).

analysis of a steel-framed building by continuously applying a seismic excitation, buoyant force, and tsunami force in a single simulation was conducted. The validity of the fluid analysis is discussed by comparing the result with that of an analysis conducted by applying an estimated wave force.

There were also some possibilities that the flow of debris such as ships, cars, and containers may have caused some destructive impact and additional damage to buildings [1]. Therefore, evacuation buildings should be designed not only to withstand seismic excitations and tsunami waves but also to cope with impacts caused by debris. A continuous simulation with some debris collided after the application of wave forces is also described in this chapter.

2. Fluid analysis using stabilized FEM

A numerical code [2] using stabilized FEM based upon the volume of fluid (VOF) method, which indirectly expresses a free-surface shape by function values, was adopted for the fluid analysis. A hybrid parallel computing method was implemented in this code to drastically reduce the computational time and memory resources to cope with large-scale simulations. This method combined a region-partitioning method communicated with message passing interface (MPI) [3] and parallel threads using OpenMP [4]. The code had already been validated by comparing the results with a concrete fracture experiment under tsunami flow conducted in a large-scale testing flume at the Port and Airport Research Institute [5].

2.1. Numerical model

A numerical model with a region of 240 m in length, 180 m in width, and 80 m in height, as shown in **Figure 2**, was constructed. Two types of buildings without any openings (reduction coefficient $\gamma = 1.00$) and with openings ($\gamma = 0.52$ when the inundation height = 8.0 m), as shown in **Figure 3**, were subdivided with finite element meshes. Here, the reduction coefficient γ is

http://dx.doi.org/10.5772/intechopen.76602

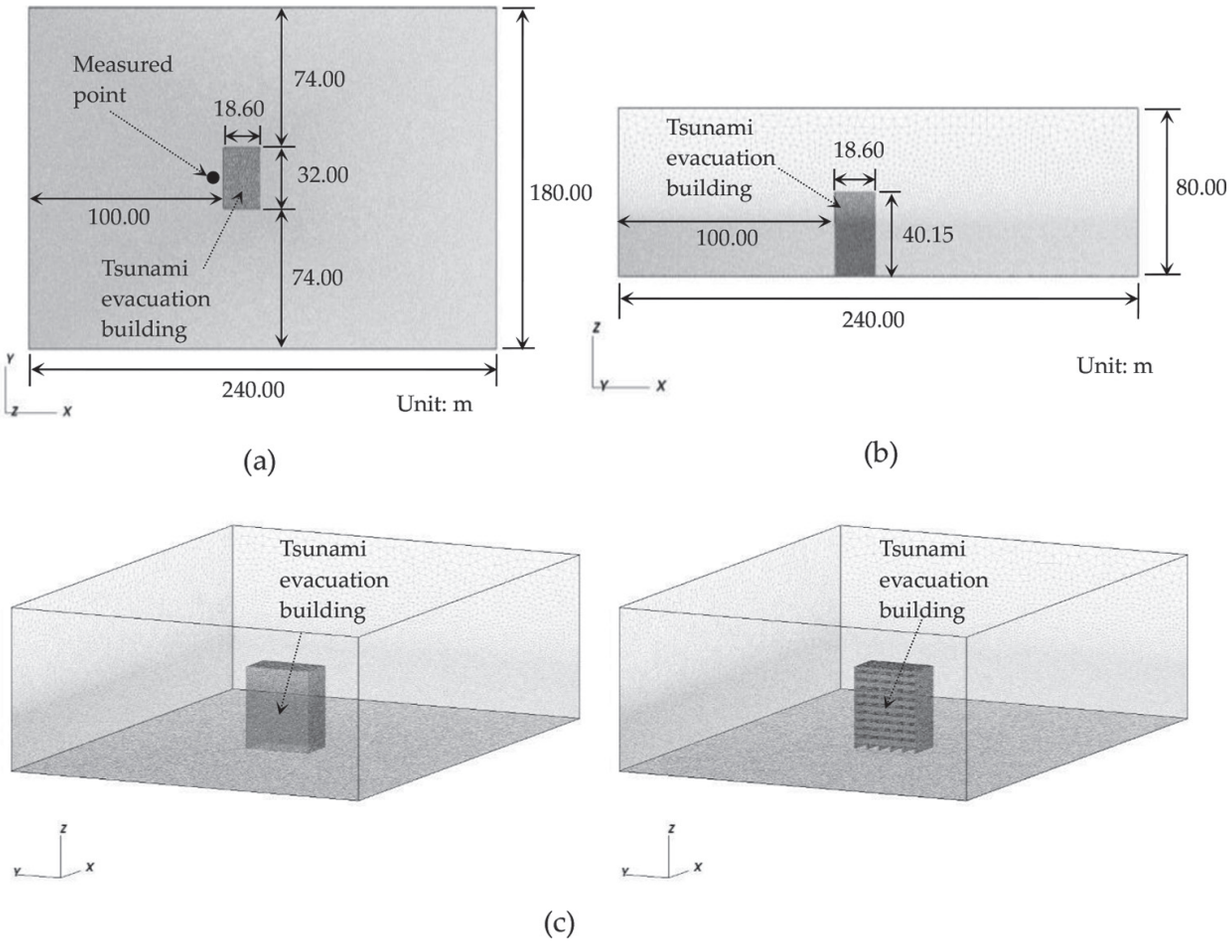

Figure 2. Global view of numerical models (a) Upper view, (b) Side view, (c) Bird's-eye view [left: model without openings ($\gamma = 1.00$), right: model with openings ($\gamma = 0.52$)].

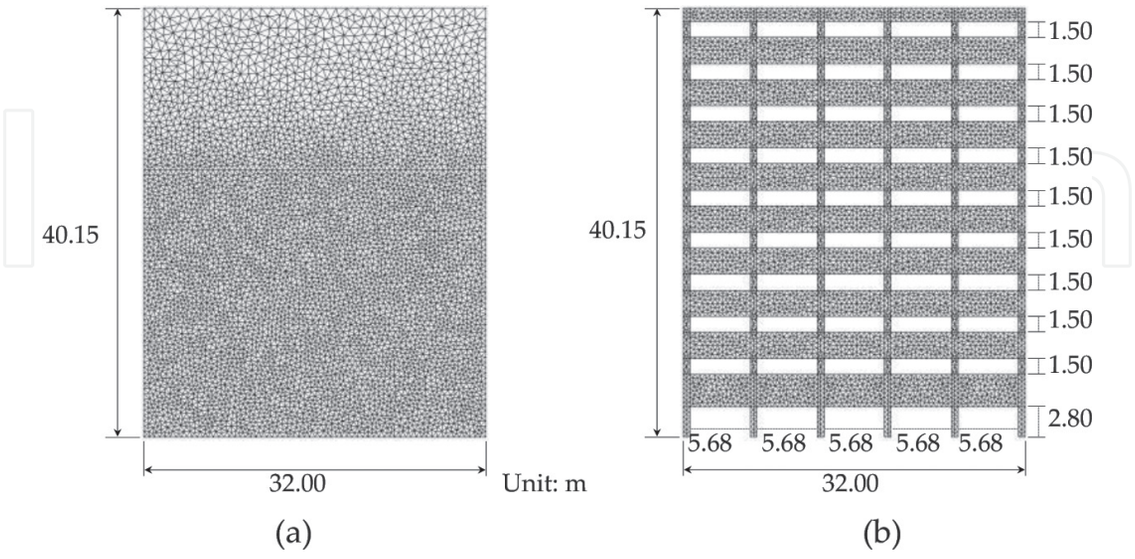

Figure 3. Numerical models of tsunami evacuation building (front view) (a) Model without openings ($\gamma = 1.00$), (b) Model with openings ($\gamma = 0.52$).

defined as the ratio of the projection area of walls to all projection areas including walls and openings under the waterline.

The building with openings was designed for evacuation uses in [6] and was 10 stories high, with 40.15 m of height and 32.00 m of width. The buildings were modeled as rigid bodies that allowed no deformation, and the openings were assumed to be located at the window parts. These models were all subdivided with tetrahedron elements, with the distances between nodes fixed at approximately 0.5 m under the waterline and around the building. The total number of nodes and elements were approximately 3.0 and 17 million for the model without openings, and 3.7 and 21 million for the model with openings, respectively.

2.2. Numerical conditions

Figure 4 shows the boundary condition for the fluid analysis. Fluid (seawater) flows into the area from the lower left corner, and air flows out from the upper right corner freely without any traction. A slip condition assuming no friction between the fluid and wall surface was selected for other areas of the walls. Three cases with the same upstream depth of 8.0 m and different flow velocities, as listed in **Table 1**, were simulated. Here, we define the upstream depth as the inundation height at a location far away from the building, as shown in **Figure 5**. The density and viscosity coefficient of seawater were fixed at 1027 kg/m^3 and 1.0 × 10^{-3} Pa·s, and those of air were fixed at 1.293 kg/m^3 and 1.8 × 10^{-5} Pa·s, respectively.

The time increment was set to 0.01 s, and a duration of 30 s was simulated using PC cluster parallel computers (3.33GHz CPU, 48GB RAM) to take full advantage of the hybrid parallel computing method. The computational time for the model without openings, for example, was about a day when using 96 parallel processors (8 nodes with 12 processors per node).

2.3. Numerical results

The shape of the flow surface and the pressure distribution computed at the front of the building for Case 3 are shown in **Figure 6** for the model without openings and in **Figure 7** for the model with openings. One can observe the inflow and propagation of the tsunami wave and the impact to the front of the building. The complex free-surface shape owing to amplification of

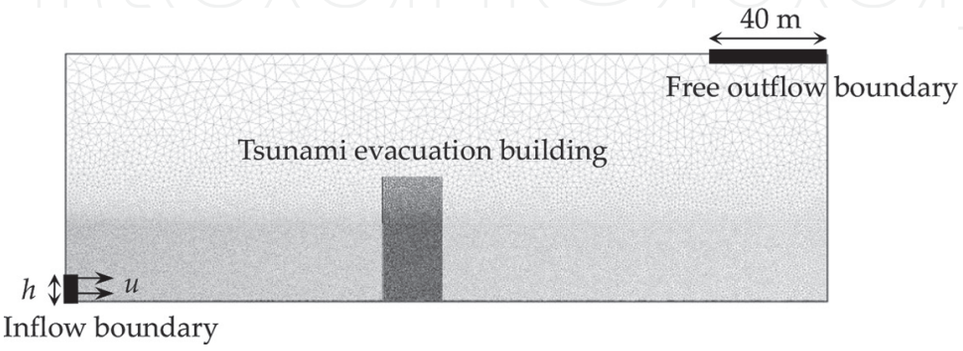

Figure 4. Boundary condition.

http://dx.doi.org/10.5772/intechopen.76602

	Upstream depth (h) [m]	Flow velocity (u) [m/s]	Froude number (F_r)
Case 1	8.0	6.0	0.67
Case 2	8.0	9.0	1.00
Case 3	8.0	12.0	1.35

Table 1. Analyzed cases.

the wave height by short reflected waves, for example, appears to be well simulated. The seawater flowing in and out of the openings can be observed in **Figure 7** for the model with openings.

The inundation height at the front of the building, therefore, becomes lower compared to that of the case without openings. The difference can also be confirmed in **Figure 8**, where the inundation heights for three cases are compared between two models. The peak heights of the waves increase sharply for the model without openings, while the heights are suppressed for the model with openings. A wide area at the lower part of the building is highly pressurized in case of the former, but the pressure is significantly reduced in case of the latter as seawater flows into the building.

The mean velocities of flow at the front of the buildings are shown in **Figure 9**. These data and the inundation heights in **Figure 8** are computed at the location shown in **Figure 2(a)** (5.0 m away from the front surface of the building). The peak velocities reach over 15 m/s in all cases; this is higher than the initial inflow velocity. The velocity quickly decreases to 0 m/s if there are no openings. On the other hand, the velocity does not reduce as much if there are openings into which the seawater can flow.

The tsunami wave forces acting on the front surface of the buildings are shown in **Figure 10**. These are calculated from the pressure data shown in **Figures 6** and **7**. Short-term impulsive forces first appear in all cases for the model without openings, followed by long stationary forces. The peak values of the impulsive forces for Cases 1, 2, and 3 are approximately 25, 40, and 60 MN, respectively, and the stationary forces for those are approximately 20, 30, and 40 MN, respectively. On the other hand, the impulsive forces do not clearly appear in all cases for the model with openings, where the values are constant at approximately 10 MN, 15 MN, and 20 MN in Cases 1, 2, and 3, respectively. These results clearly show the effect of wave force reduction by making large openings at the lower parts of the buildings.

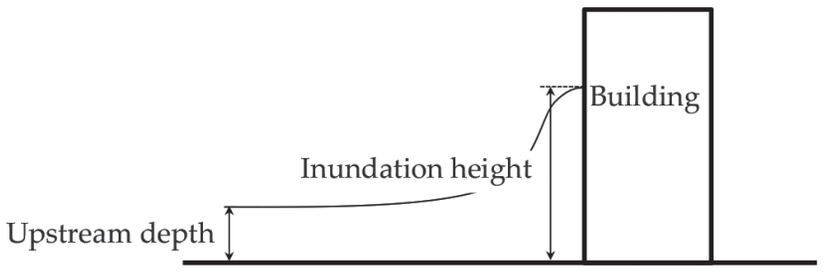

Figure 5. Upstream depth and inundation height in front of the building.

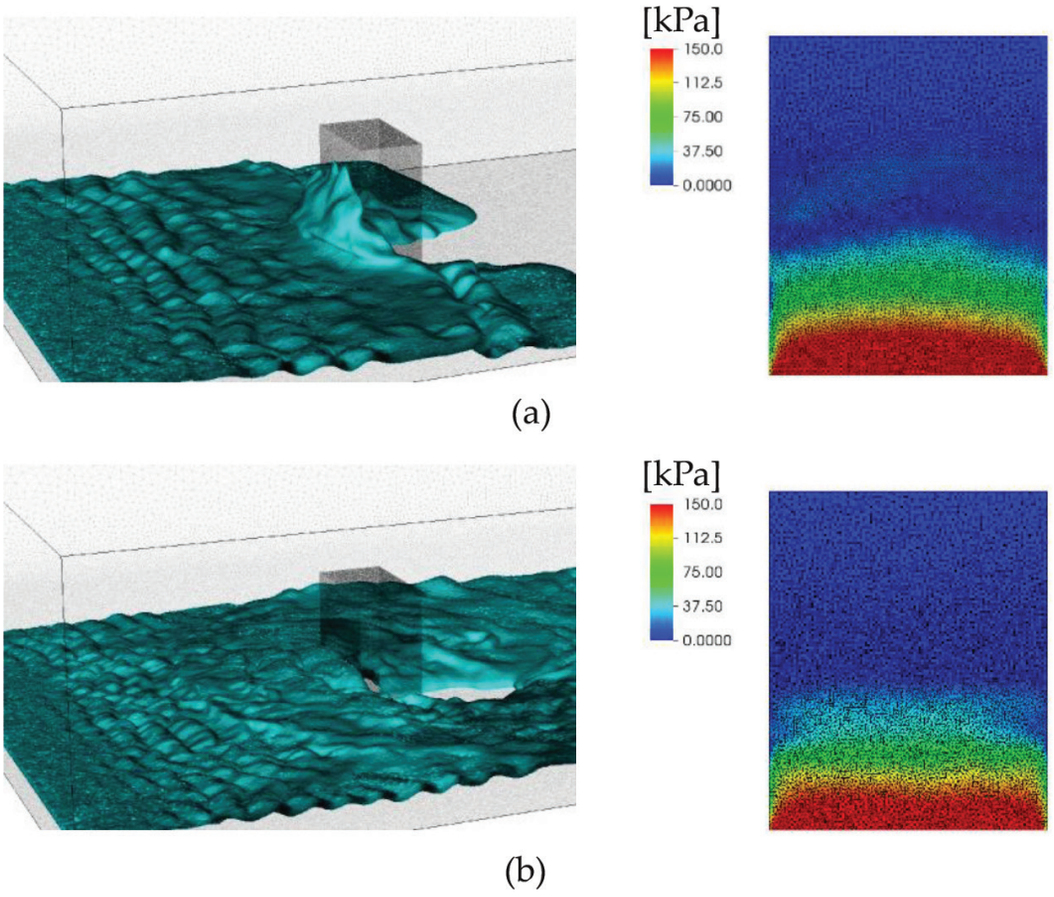

Figure 6. Shape of flow surface (left) and pressure distribution on the front surface of the building (right) [Case 3, model without openings (γ = 1.00)] (a) 10 s, (b) 20 s.

Next, estimated wave forces calculated from inundation heights and flow velocities are compared with simulated wave forces obtained from the fluid analyses. Here, a sum of hydrostatic load F_S and drag force F_D is used as the estimated wave force, as shown in **Figure 11**, by assuming that only a stationary force with an inundation height and a fluid velocity independent of the time duration acts on a building. The hydrostatic load is distributed in a triangular shape and the drag force in a rectangular shape, as shown in the figure, to the surface of the building. These forces are calculated using the following equations:

$$F_S = \gamma \rho_S g B \int_{z_1}^{z_2} (h - z) dz \tag{1}$$

$$F_D = \frac{1}{2} \gamma \rho_S C_D u^2 A \tag{2}$$

Here, ρ_s is the density of seawater, g is the gravitational acceleration, B is the width of the pressurized surface, z_1 is the minimum and z_2 is the maximum height of the pressurized surface, h is the inundation height, C_D is the drag coefficient, u is the relative velocity between the flow and the object, and A is the area of the pressurized surface. The reduction in the wave force owing to openings is considered here, using the reduction coefficient γ as in the provisional guideline [7].

http://dx.doi.org/10.5772/intechopen.76602

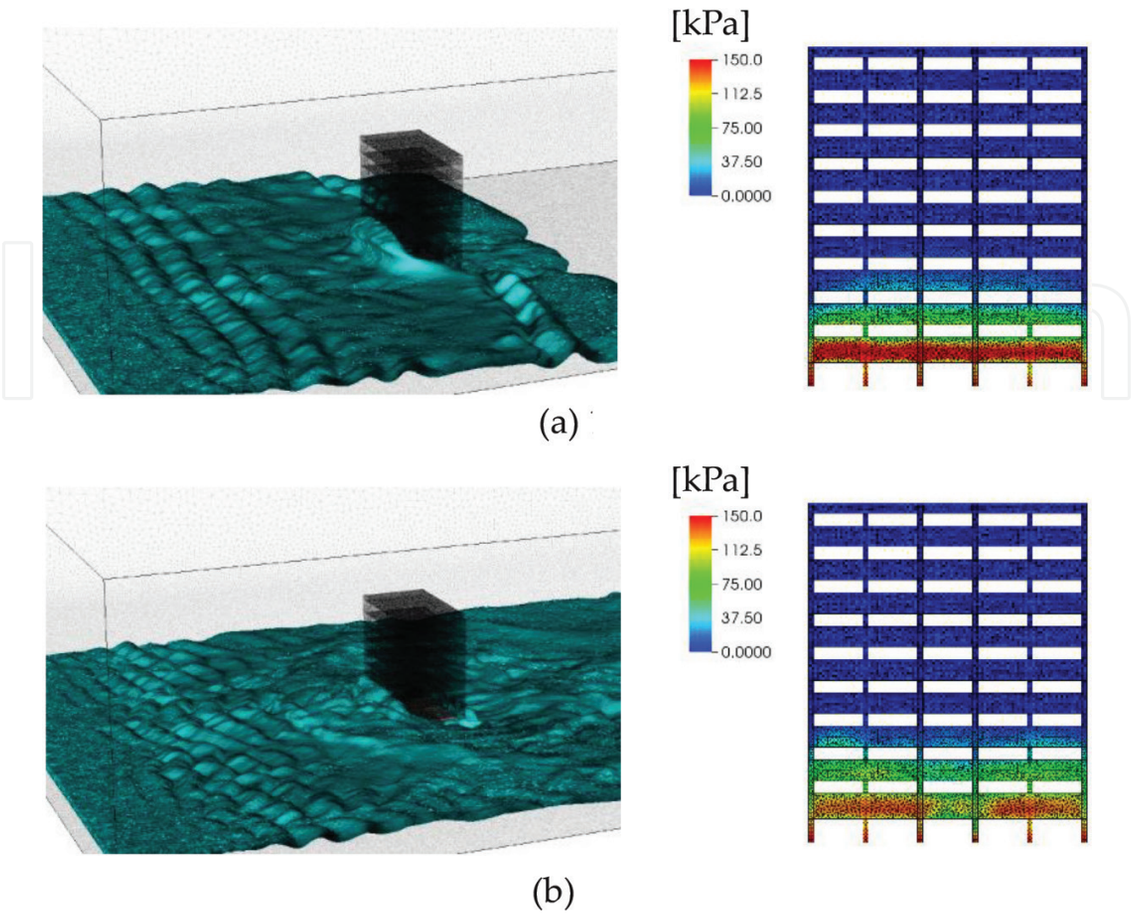

Figure 7. Shape of flow surface (left) and pressure distribution on the front surface of the building (right) [Case 3, model with openings (γ = 0.52)] (a) 10 s, (b) 20 s.

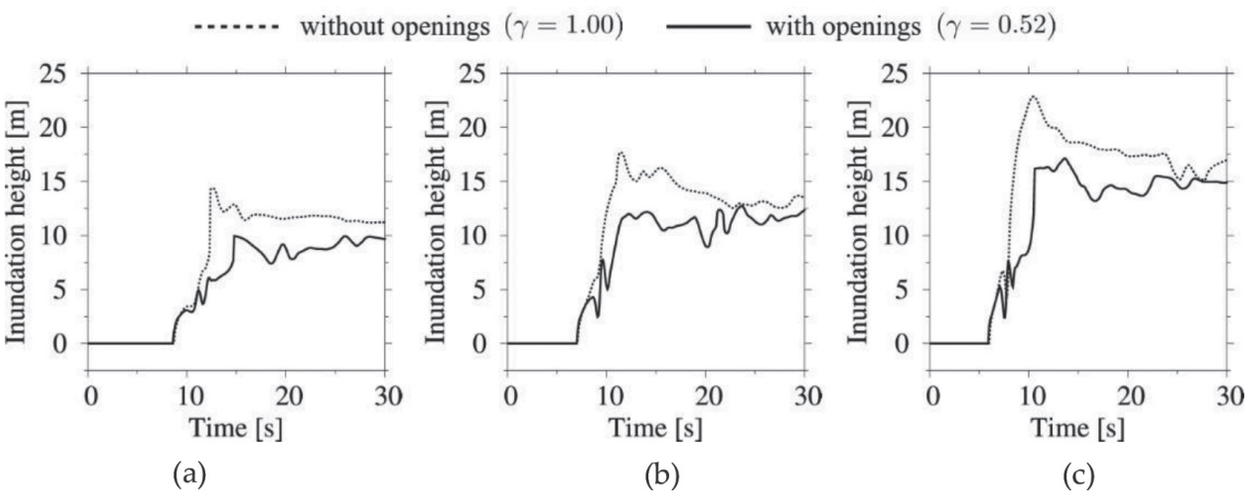

Figure 8. Inundation heights in front of the building (a) Case 1, (b) Case 2, (c) Case 3.

Drag coefficients are likely to vary depending on the shape of a building, particularly if considering the presence of openings. To see the differences, the drag coefficients are calculated backward from the wave forces shown in **Figure 10** using Eqs. (1) and (2). **Figure 12** shows the

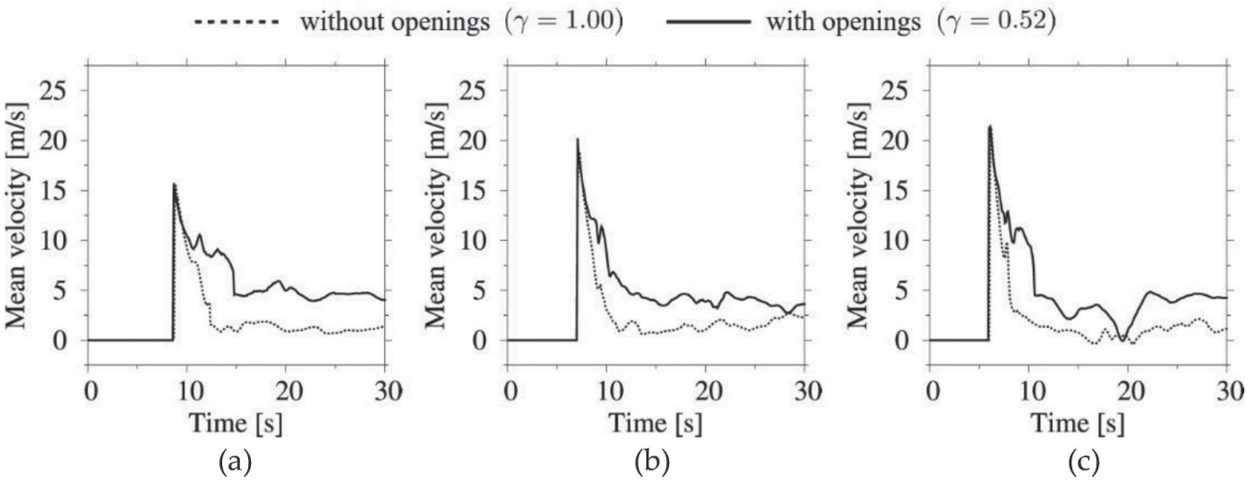

Figure 9. Mean velocities of flow in front of the building (a) Case 1, (b) Case 2, (c) Case 3.

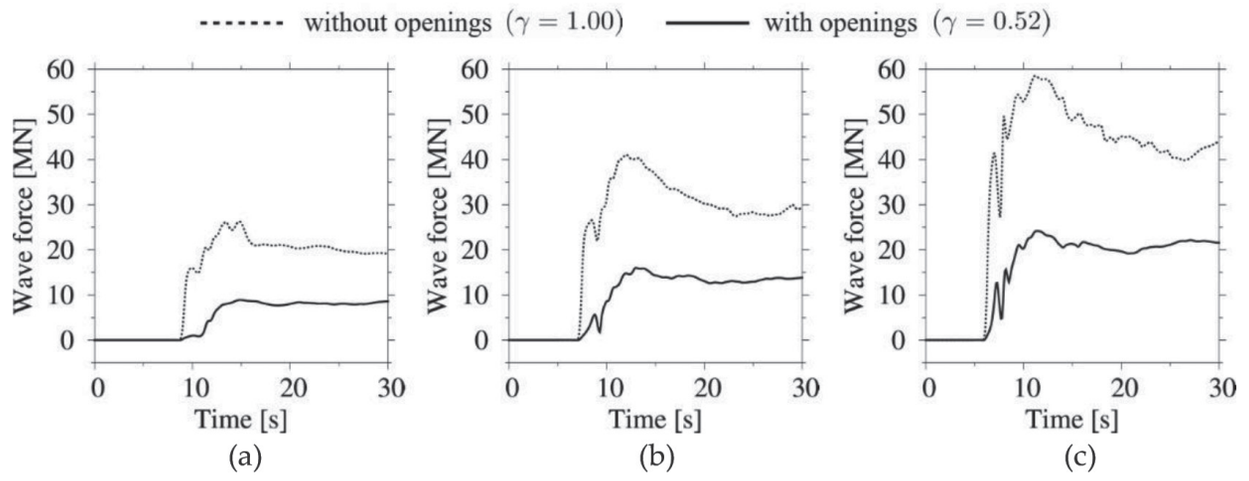

Figure 10. Tsunami wave forces acting on the front surface of the building (a) Case 1, (b) Case 2, (c) Case 3.

time histories of the obtained drag coefficients. As shown in the figures, the drag coefficients converge approximately to a value of 2.0 in all cases of γ = 1.00; the value is almost equivalent to that obtained from the hydraulic experiment [8]. Similarly, the coefficients converge approximately to a value of 1.5 in all cases of γ = 0.52. It is confirmed that the drag coefficients may be fixed to constant values depending on the shape of the building, but not depending on the inflow condition.

The estimated wave forces obtained using the above drag coefficient values (C_D = 2.0 for γ = 1.00 and C_D = 1.5 for γ = 0.52) are compared with the simulated wave forces obtained from fluid analyses. **Figure 13** shows a comparison between both forces in the case of γ = 1.00 and **Figure 14** in the case of γ = 0.52. The time histories of the estimated wave forces were obtained by applying a hydrostatic load in one step and a drag force incrementally for 1 s.

The estimated wave forces roughly approximate the stationary forces in both figures; however, they do not replicate the impulsive components that appear in **Figure 13**. Therefore, the

http://dx.doi.org/10.5772/intechopen.76602

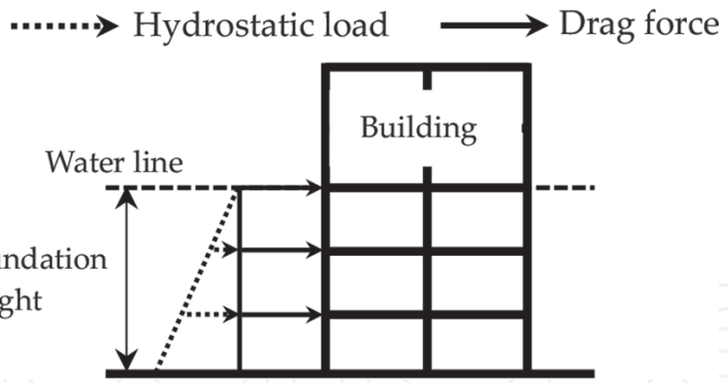

Figure 11. Schematic diagram of hydrostatic load and drag force acting on the surface.

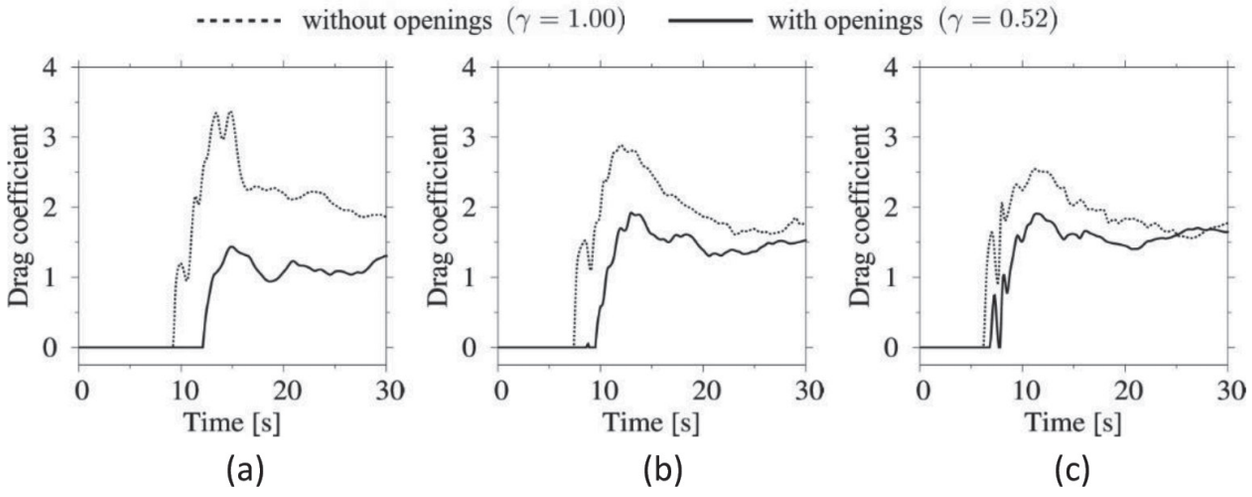

Figure 12. Time histories of drag coefficients (a) Case 1, (b) Case 2, (c) Case 3.

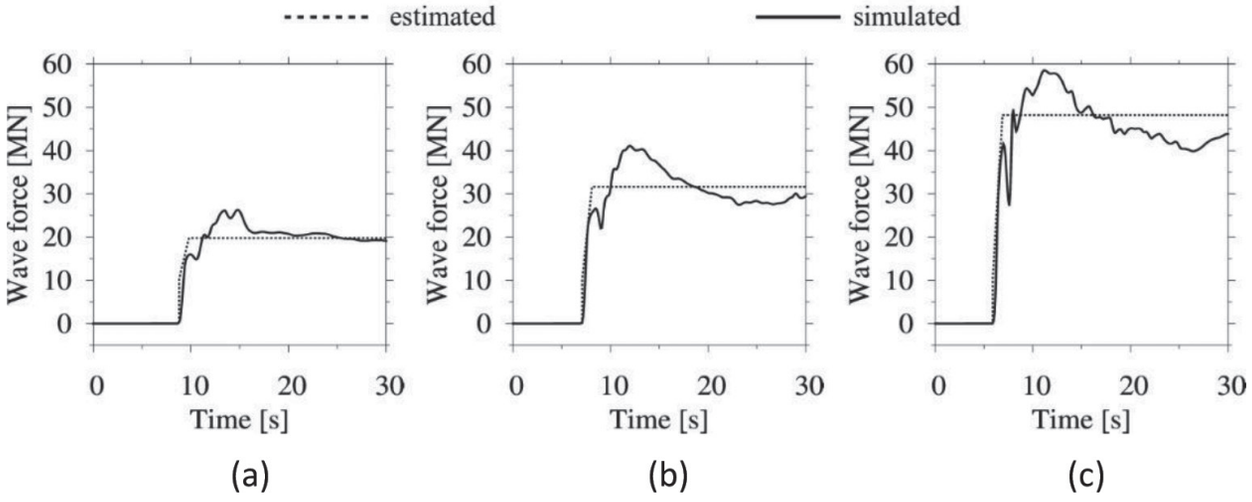

Figure 13. Comparison between estimated and simulated wave forces [model without openings (γ = 1.00)] (a) Case 1, (b) Case 2, (c) Case 3.

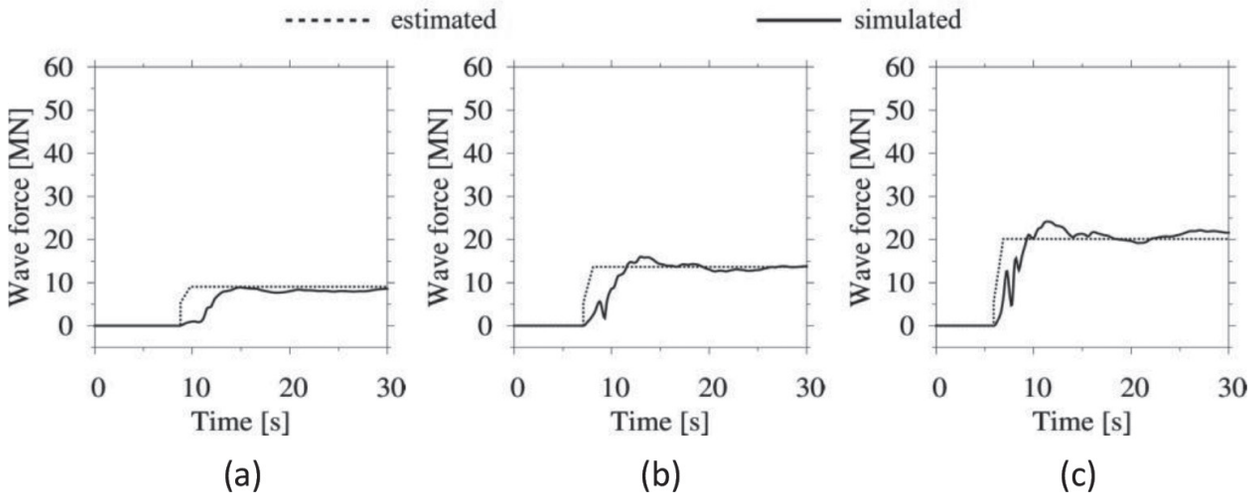

Figure 14. Comparison between estimated and simulated wave forces [model with openings (γ = 0.52)] (a) Case 1, (b) Case 2, (c) Case 3.

estimated wave forces can only be applied to cases when consideration of impulsive waves is not required, and the fluid analysis becomes helpful if a more detailed consideration of wave forces is required.

3. Structural analysis of tsunami evacuation building considering tsunami wave force

A one-way coupling analysis of the fluid and structure was conducted using the simulated wave force obtained from the fluid analysis. The result was compared with that obtained using the estimated wave force, and the validity of the fluid analysis was examined. The behavior of the building was simulated using the adaptively shifted integration (ASI)-Gauss code [9, 10].

3.1. Numerical model

The simulation target of the one-way coupling analysis was the same evacuation building considered in the previous section. A numerical model for the structural analysis is shown in **Figure 15**. The model consists of columns, beams, floors, foundation beams, and piles, all constructed with linear Timoshenko beam elements. Nonstructural walls such as precast curtain walls were not modeled. The building was a 10-story steel-framed building with a total height of 40.15 m, a total width of 32.00 m, and floor heights of 3.95 m (excluding the first floor, which is 4.60 m), designed with a base shear coefficient of 0.16.

The columns were square steel pipes made of BCP325, and the girders were H-type steel beams made of SN490B. Young's modulus, Poisson's ratio, yield stress, and density were 205 GPa, 0.3, 325 MPa, and 7.85×10^{-6} kg/mm^3, respectively. H-type steel beams made of SN490B were also used for the binders; the depth, total width, web width, and flange width were 450, 200, 9, and 14 mm, respectively. The concrete piles were approximated by fixing the length to 3 m

http://dx.doi.org/10.5772/intechopen.76602

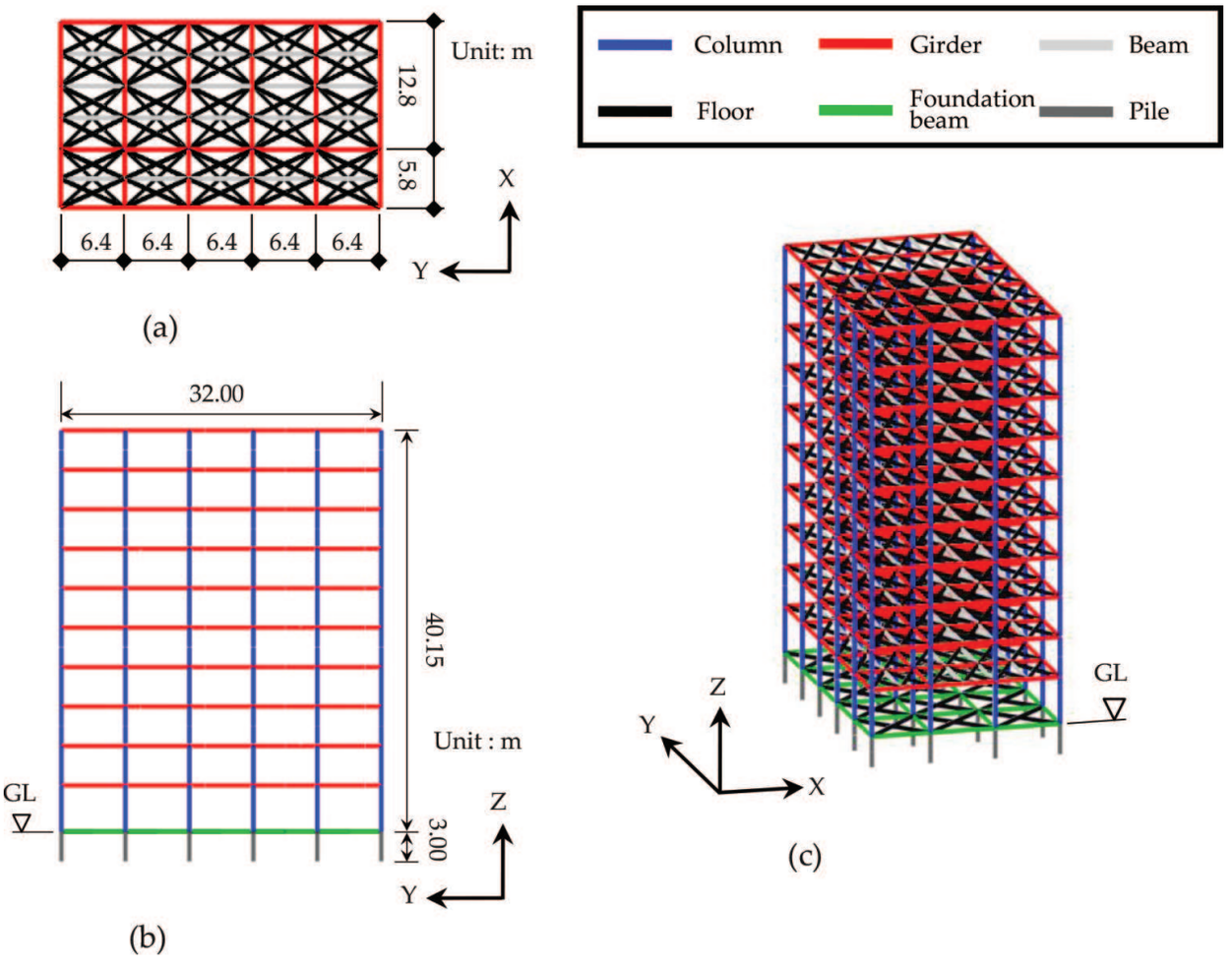

Figure 15. Numerical model of tsunami evacuation building (a) Upper view, (b) Front view, (c) Bird's-eye view.

with a weight of 1.32 MN each, while the real piles were 30 m long with circular sections of 2 m in diameter. Each section was replaced with a square section of the same area to simulate the same strength. Elastic elements were used for the floors, piles, and foundation beams.

The floor loads were set to 540 kgf/m^2 on the first to tenth floors and 670 kgf/m^2 on the roof. The weights of nonstructural components were converted to densities and added to the elements constituting the beams and floors. The total weight of the building reached 58.90 MN, which was the same value shown in [6]. The damping ratio of the model was 2%. The total numbers of elements and nodes were 3720 and 2350, respectively. The natural periods (1.36 s in the X direction and 1.37 s in the Y direction) and ultimate horizontal resistance forces of the model showed good agreement with the values in [6].

3.2. Load conditions

A 100% K-NET Sendai wave observed during the Great East Japan Earthquake was used as the input wave. **Figure 16** depicts the three-dimensional components of the input wave, and **Figure 17** shows its acceleration response spectrum. A numerical analysis was conducted

from t = 0 to 150 s, including the two peaks observed in the seismic wave. The predominant periods of the K-NET Sendai wave were 0.65 s in the East-West (EW) and North-South (NS) directions and 0.15 s in the up-down (UD) direction.

The buoyant force F_B acting vertically upward in the building under the waterline is calculated using the following equation [7]:

$$F_B = \rho_s V g \tag{3}$$

Here, V is the volume of water removed by the building. For the model without openings under the waterline, the entire volume of the model underwater was used as V, and the buoyant forces were applied only to the nodes on the perimeter under the waterline. For the model with openings under the waterline, the summed volume of columns, beams, floors, and air pockets under the floors was used as V, and the buoyant forces were applied to all nodes inside the model under the waterline as the seawater flowed into the building.

The estimated wave force, which is a summation of the hydrostatic load and drag force, as shown in Eqs. (1) and (2), and simulated wave force obtained by fluid analysis were used as the horizontal forces applied to the building. The wave forces were applied to the nodes distributed on the surface of the model under the waterline.

3.3. Numerical results

A seismic response analysis was first conducted by applying the K-NET Sendai seismic wave from t = 0 to 150 s. Then, as the next phase, the tsunami wave force was applied to the building model. For the estimated wave force, both the hydrostatic load and buoyant force were applied statically in one step, followed by a dynamic, incremental application of the drag force for 1 s. For the simulated wave force, the buoyant force was applied statically in one step before dynamically applying the time history data of the wave force.

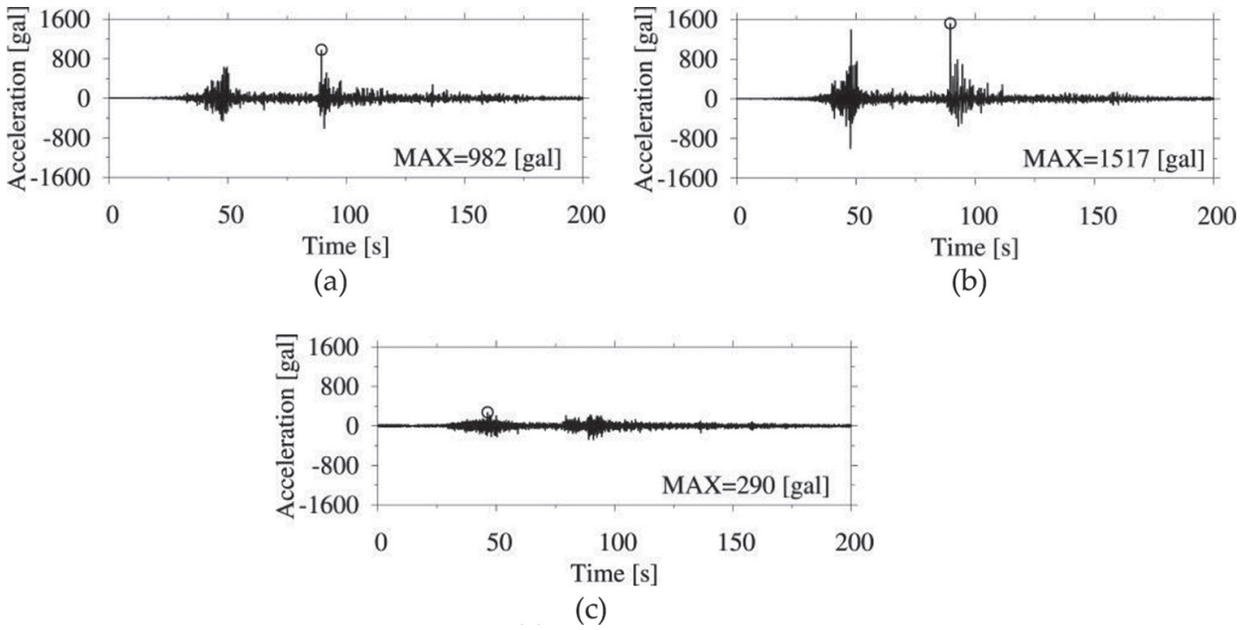

Figure 16. K-NET Sendai seismic wave (a) EW direction, (b) NS direction, (c) UD direction.

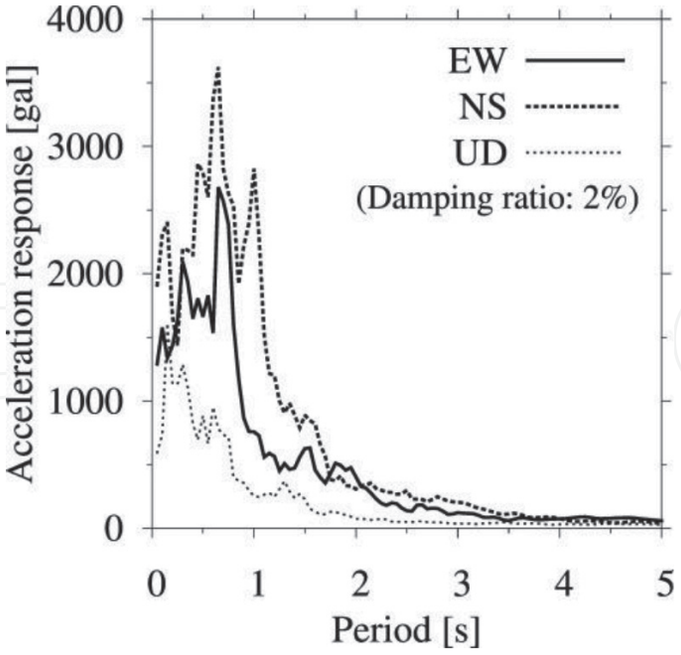

Figure 17. Acceleration response spectrum of K-NET Sendai seismic wave.

3.3.1. Seismic response analysis

The behavior of the building during seismic excitation is shown in **Figure 18**. The elements are colored according to yield function values f_y, which indicate the material properties of the elements: blue, for example, indicates that the element is totally elastic, while red indicates that the element is yielded. The yield condition is expressed as follows:

$$f = \left(\frac{M_x}{M_{x0}}\right)^2 + \left(\frac{M_y}{M_{y0}}\right)^2 + \left(\frac{N}{N_0}\right)^2 - 1 \equiv f_y - 1 = 0 \tag{4}$$

Here, M_x, M_y, and N are the bending moments around the x-axis, y-axis, and axial force, respectively. Terms with the subscript 0 are values that result in a fully plastic section in an element if they act on the cross section independently.

As shown in **Figure 18**, comparatively large sectional forces appear in the building as it deforms largely at the first peak of the input wave (t = 46.0 s) and at the second (t = 90.5 s). The residual and maximum interstory drift angles are shown in **Figure 19**. The maximum interstory drift angle reached nearly 1/50 rad at the seventh floor and nearly or over 1/100 at other floors. However, the residual interstory drift angle showed merely 1/400 rad at most on the third floor, and the damage to the building was very small.

3.3.2. Structural analysis under tsunami wave force

First, the estimated wave force calculated from the most severe condition observed on March 11, 2011, according to [11], was applied to the building. The most severe condition owing to the tsunami was observed at Onagawa-cho (**Figure 20**), with an inundation height of 15.0 m and a wave velocity of 9.47 m/s. Here, the reduction coefficient γ owing

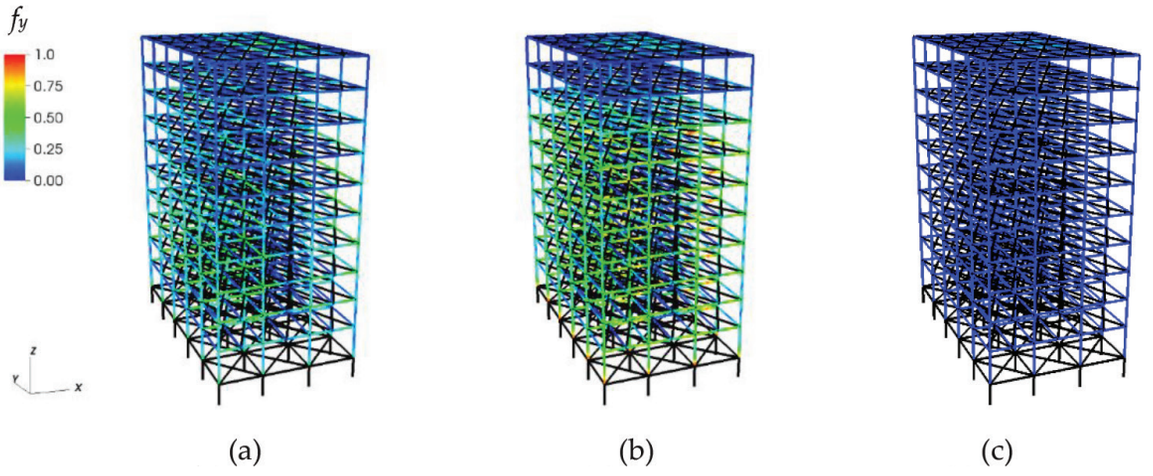

Figure 18. Behavior of the building during seismic excitation (a) 46.0 s, (b) 90.5 s, (c) 150.0 s.

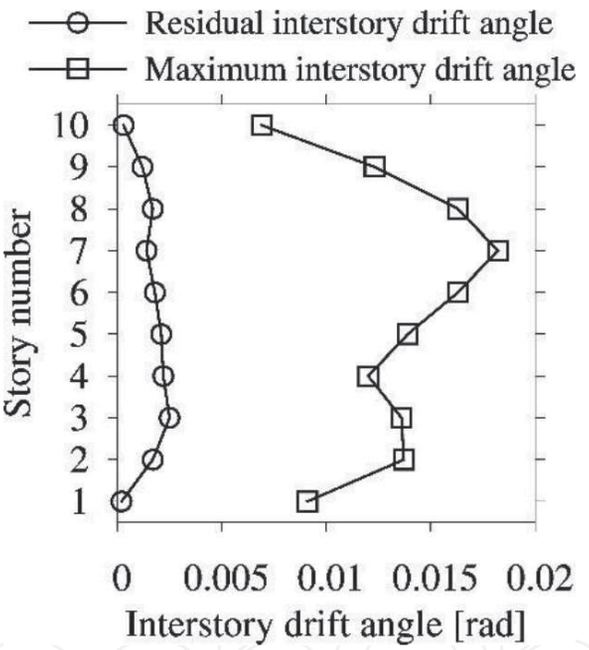

Figure 19. Residual and maximum interstory drift angles.

to openings can be calculated as 0.58 at this inundation height. **Figures 21** and **22** show the behaviors of the buildings under this condition. The building washed away, as a consequence, after the elements on the first floor fractured consecutively from the surface of the building in the case of the model without openings (**Figure 21**). By contrast, none of the elements fractured even under this severe condition in the case of the model with openings (**Figure 22**).

Next, the numerical results are compared between the estimated and simulated wave forces shown in **Figures 13** and **14**. The interstory drift angles on the first floor obtained under both wave forces are plotted in **Figure 23** for the case of γ = 1.00 and in **Figure 24** for the case of

Figure 20. View of disaster site (Onagawa-cho, 28 months after the event) (photo by Daigoro Isobe).

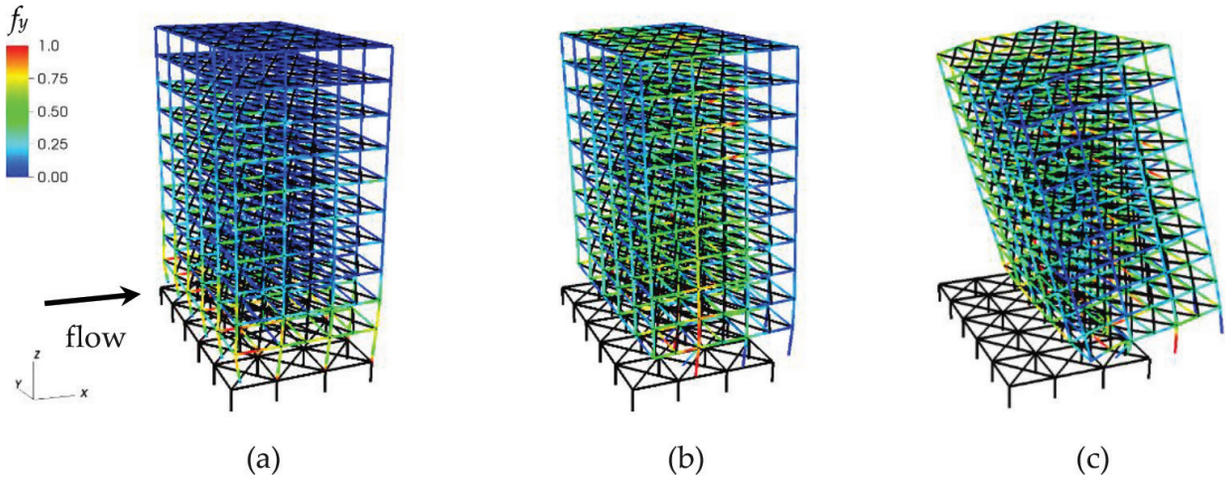

Figure 21. Behavior of the building when tsunami wave force is applied [model without openings (γ = 1.00)] (a) 0.8 s, (b) 1.2 s, (c) 1.9 s.

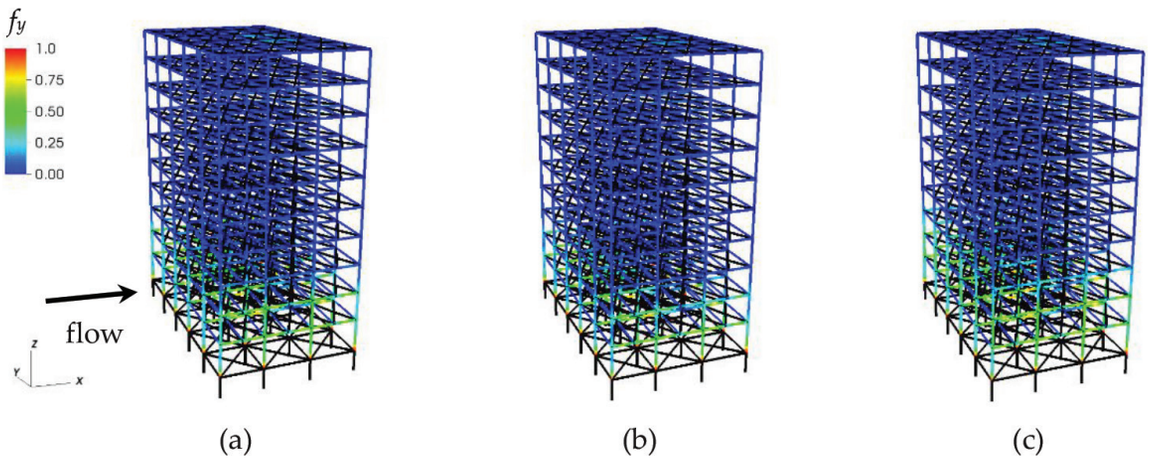

Figure 22. Behavior of the building when tsunami wave force is applied [model with openings (γ = 0.58)] (a) 0.8 s, (b) 1.2 s, (c) 1.9 s.

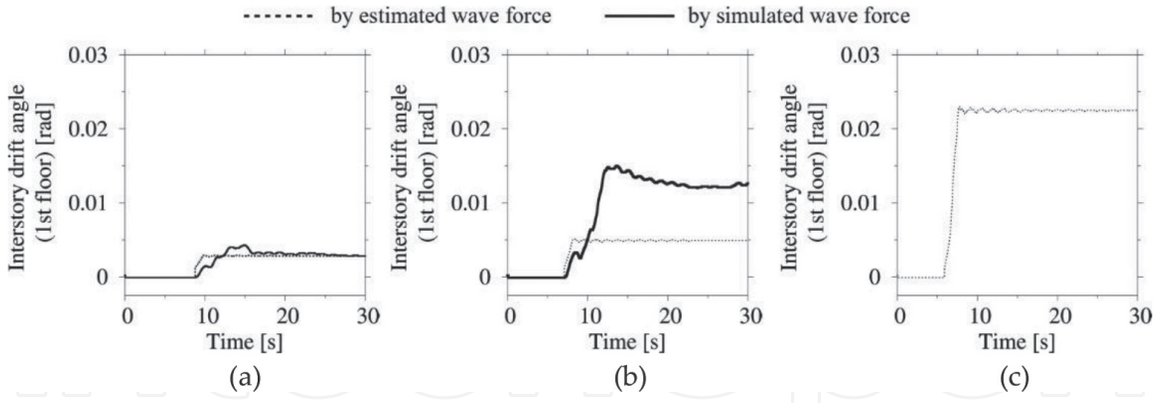

Figure 23. Time histories of interstory drift angle on first floor [model without openings (γ = 1.00)] (a) Case 1, (b) Case 2, (c) Case 3.

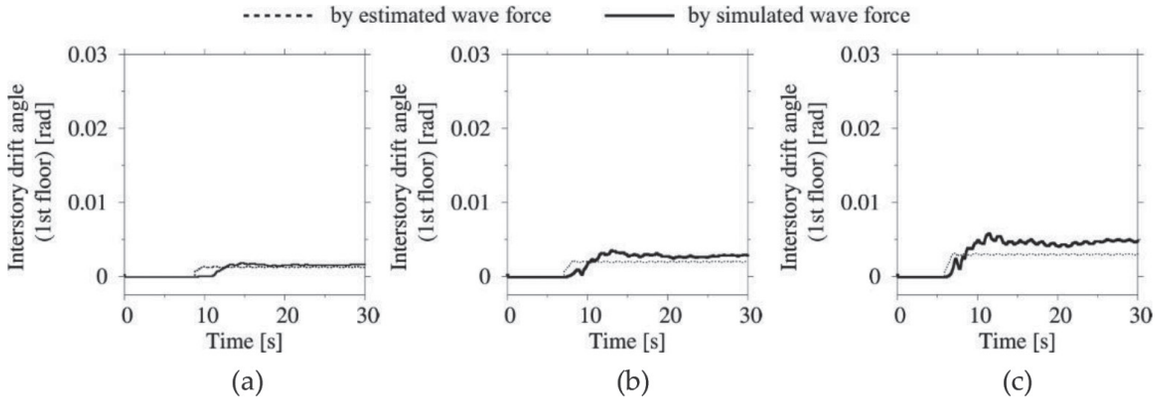

Figure 24. Time histories of interstory drift angle on the first floor [model with openings (γ = 0.52)] (a) Case 1, (b) Case 2, (c) Case 3.

γ = 0.52. Here, the inundation height is 8.0 m, as in Section 2. The washed-away cases are omitted in these figures. Large differences can be seen, especially in **Figure 23(b)** and **(c)**, between these results under the estimated and simulated wave forces.

The interstory drift angle was suppressed to 1/200 rad under the estimated wave force in Case 2; however, it exceeded 1/100 rad when the simulated wave force was applied. The building even washed away in Case 3, when the simulated wave force was applied. There seem to be no significant differences, on the other hand, between both results in all cases shown in **Figure 24**. Furthermore, the angle is significantly suppressed compared to that in **Figure 23**, which shows a large contribution of openings at lower floors to damage reduction.

4. Debris impact analysis of tsunami evacuation building

Finally, an initial velocity was applied to some container boxes that mimicked the debris owing to the tsunami. An impact analysis was conducted following the previous analysis applying the tsunami wave force.

4.1. Numerical model and conditions

A container box made of SS400 steel with a weight of 24.0 t, length of 6.0 m, and width and height of 2.5 m, was used as the debris model. The container box model and a global view of the numerical models are shown in **Figure 25**. Six container boxes with drafts of 1.25 m were

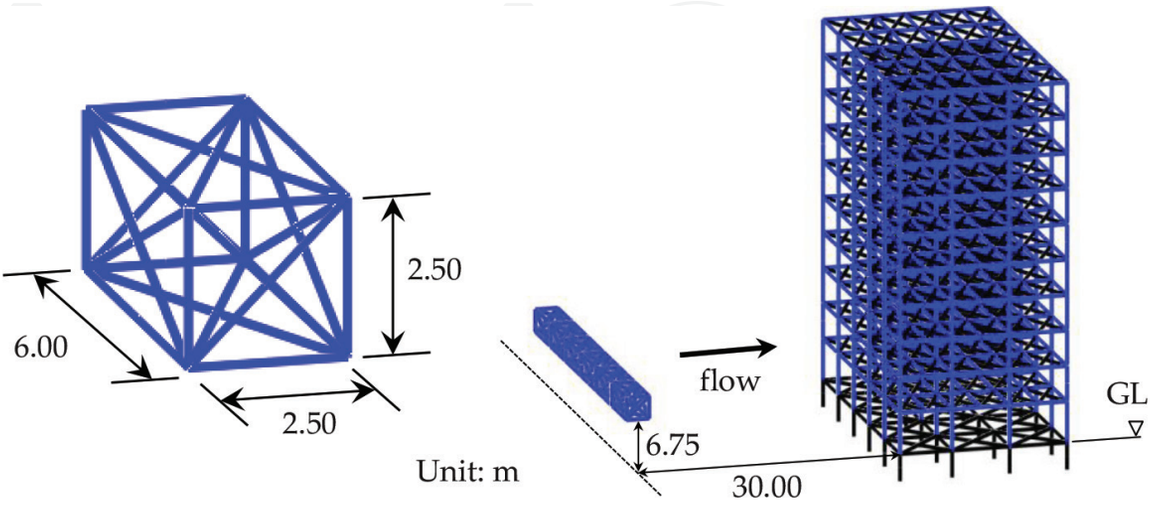

Figure 25. Container box model and global view of numerical models.

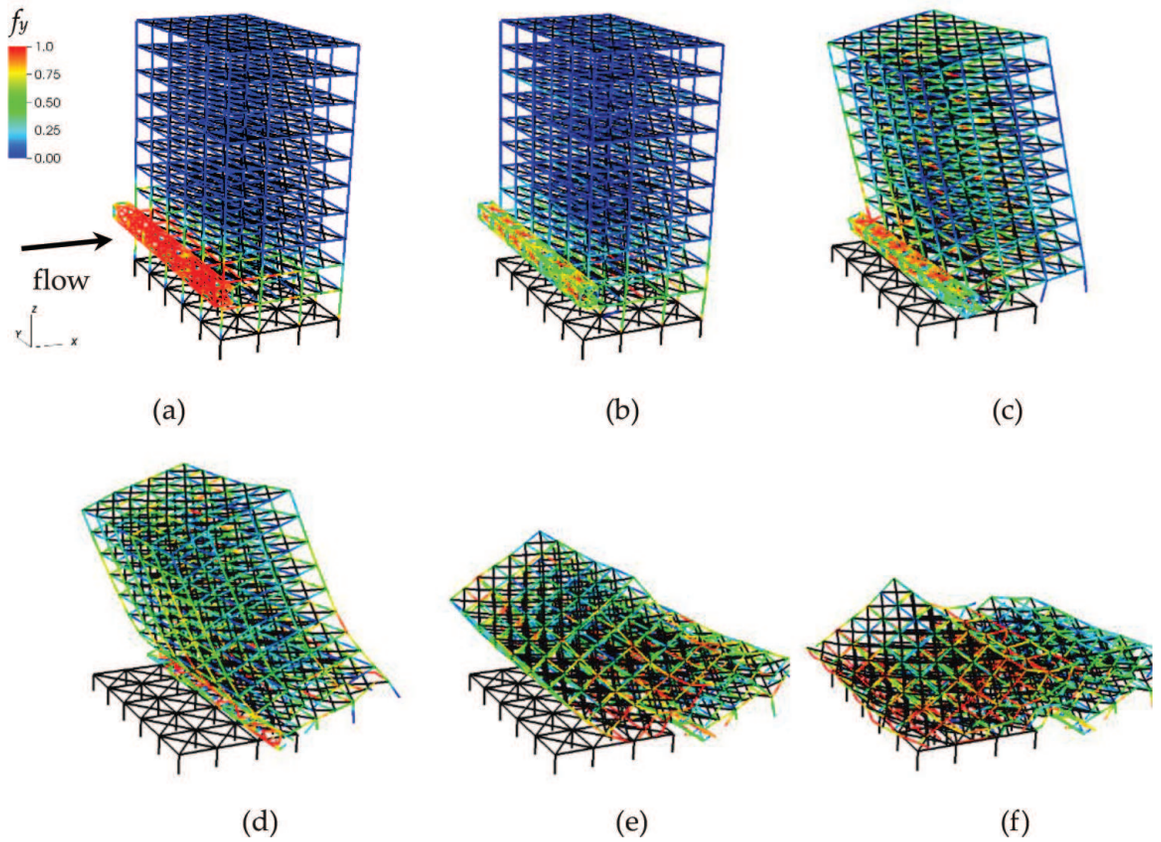

Figure 26. Behavior of the building during debris collision a) 0.0 s (on impact), (b) 0.8 s, (c) 2.3 s, (d) 3.2 s, (e) 4.2 s, (f) 4.7 s.

placed side by side at a location 30.0 m away from the front surface of the building. Only a drag force was applied to the boxes, and the estimated wave force of Case 3 and γ = 1.00 shown in **Figure 13(c)** was applied to the building. An initial velocity equivalent to the tsunami flow was given to the container boxes in the direction of the building to simulate the impact phenomena.

4.2. Numerical result

Figure 26 shows the behavior of the building owing to the impact of the tsunami debris. The container boxes collide near the beam-column joint sections of the second and third floors, causing ultimate material failures to columns and beams around the impact point. The shock wave rapidly propagating from the impact point can also be observed. The relative velocity between the debris and tsunami flow increases when the debris reduces its velocity in front of the building. Then, a much larger drag force is applied to the debris and thereby to the building itself. Member fractures initiate at the front columns of the first floor and propagate progressively to the inside. Finally, the building collapses and is washed away.

5. Conclusions

In this chapter, a fluid analysis using a stabilized FEM was described, and the differences of the free-surface shapes and tsunami wave forces between models with and without openings were explained. A wide area at the lower part of the building was highly pressurized for the model without openings, but the pressure was significantly reduced for the model with openings as the seawater flowed into the building. These results clearly showed the effect of wave force reduction by making large openings at the lower parts of the buildings. However, the openings may increase the possibility of debris colliding into the building, caused by the inflow motion of seawater into the openings. Further investigation should be conducted in this field.

Next, the estimated and simulated wave forces were compared, and their limitation and validity were explained. It was shown that the estimated wave force could roughly approximate the stationary force acting on the surface of the building, while the simulated wave force could consider both the impulsive peak and the stationary force. The behaviors of the building under both wave forces were compared, and the effect of the impulsive wave on the building damage was confirmed. The interstory drift angle of the building was also drastically reduced by the openings at lower floors.

Finally, a debris model constructed of six container boxes was introduced, and an impact analysis of the building was conducted. The impact phenomena and damage to the building were practically simulated. However, a change in the flow channel geometry according to current changes near the openings should be simulated in future investigations to consider a more precise flow path of tsunami debris. The demand for a more advanced, two-way coupling analysis between the fluid and structure is now growing.

Acknowledgements

This research was partially supported by the Grants-in-Aid for Scientific Research (No. 17H02057) of the Japan Society for the Promotion of Science (JSPS). The authors would also like to acknowledge the contribution of Mr. Hiroaki Ogino, a former graduate student of the University of Tsukuba, to the numerical analyses.

Author details

Daigoro Isobe* and Seizo Tanaka

*Address all correspondence to: isobe@kz.tsukuba.ac.jp

University of Tsukuba, Tsukuba-shi, Ibaraki, Japan

References

[1] National Institute for Land and Infrastructure Management (NILIM). Report on field surveys and subsequent investigations of building damage following the 2011 off the Pacific coast of Tohoku earthquake. Technical Note of National Institute for Land and Infrastructure Management. No. 636; Building Research Data No. 132; 2011 (in Japanese)

[2] Tanaka S, Sun F, Hori M, Ichimura T, Wijerathne MLL. Large-Scale Failure Analysis of Reinforced Concrete Structure by Tsunami Wave Force. In: 15th World Conference in Earthquake Engineering (15WCEE), CD-ROM. Lisbon, Portugal; 2012

[3] Gropp W, Lusk E, Skjellum A. Using MPI: Portable Parallel Programming with the Message-Passing Interface. 3rd ed. Cambridge, MA: The MIT press; 2014

[4] Chapman B, Jost G, Van der Pas R. Using OpenMP: Portable Shared Memory Parallel Programming. Cambridge, MA: The MIT press; 2008

[5] Arikawa T. Structural Behavior Under Impulsive Tsunami Loading. Journal of Disaster Research. 2009;**4**(6):377-381

[6] National Institute for Land and Infrastructure Management (NILIM). Practical guide on requirement for structural design of tsunami evacuation buildings. Technical Note of National Institute for Land and Infrastructure Management No. 673; 2012 (in Japanese)

[7] Housing Bureau, Ministry of Land, Infrastructure, Transport and Tourism. Provisional guideline on requirement for structural design of tsunami evacuation buildings based on building damage owing to tsunami following the 2011 off the Pacific Coast of Tohoku Earthquake; 2011 (in Japanese)

[8] Arnason H, Petroff C, Yeh H. Tsunami bore impingement onto a vertical column. Journal of Disaster Reserch. 2009;**4**(6):391-403

[9] Lynn KM, Isobe D. Finite element code for impact collapse problems of framed structures. International Journal for Numerical Methods in Engineering. 2007;**69**(12):2538-2563

[10] Isobe D. Progressive Collapse Analysis of Structures: Numerical Codes and Applications. Cambridge, MA: Elsevier Inc.; 2017. eBook; ISBN: 9780128130421; Paperback ISBN: 9780128129753

[11] Institute of Industrial Science, University of Tokyo. Interim report on development of building standards in tsunami hazard area, Part 2, 2011 Development and Promotion Project of Building Standards; 2011 (in Japanese)